

Constructing a Closed Road Search Model Using GIS and Satellite Data for Post-Tsunami Transportation Optimization

Shouyi Gao, *Member, IAENG*, Mitsugu Saito

Abstract—With global advancements in space exploration and research, medium- to low-resolution satellite data have become increasingly accessible for educational and research applications. Remote sensing technology plays a crucial role in various fields, including natural resource management, environmental conservation, and disaster prediction. However, satellite orbit cycles and varying climatic conditions can restrict access to high, resolution time-series images, affecting the accuracy of flood impact assessments. This study examines the use of satellite remote sensing and Geographic Information Systems (GIS), to identify tsunami-inundated areas in Miyagi Prefecture’s coastal regions after the 2011 Great East Japan Earthquake. To enhance mapping accuracy, we applied the Normalized Difference Water Index (NDWI) and the Normalized Difference Snow Index (NDSI) from Landsat 7, along with land surface temperature (LST) data from MODIS11A2, using binarized satellite images. We also employed GIS to identify road damage in inundated areas, where typical navigation tools may lack real-time accessibility data. To aid in disaster response and recovery, we explored a satellite- and GIS-based route search system for determining the shortest accessible routes in affected areas, thereby streamlining aggregate supply logistics. The objective of this study was to establish an efficient and time-saving aggregate supply network that connects quarries to critical infrastructure repair sites while estimating specific transportation times. By leveraging satellite-based route assessments and GIS integration, this approach aimed to enhance the efficiency of post-disaster logistics and supply chain management.

Index Terms—Satellite Data, GIS, NDWI, LST, NDSI, Aggregate Transportation Routes.

I. INTRODUCTION

JAPAN situated within the Pacific Ring of Fire, is highly susceptible to frequent seismic activity, resulting in devastating earthquakes and subsequent tsunami-induced inundation disasters. These events pose significant risks to coastal regions, threatening extensive damage to infrastructure and loss of human life [1]. Traditional methods for determining inundated areas typically involve ground surveys and aerial reconnaissance [2]. Although precise, ground surveys are time-consuming and resource-intensive, making them impractical for large-scale disasters. Aerial reconnaissance allows for quicker assessments but is often limited by adverse weather and deployment constraints during emergencies [3]. The visualization of inundated areas and debris accumulation is crucial for identifying passable roads following a tsunami.

Manuscript received December 23, 2024; revised June 24, 2025.

Shouyi Gao is a PhD candidate in Design and Media Technology, Graduate School of Engineering, Iwate University, Morioka, Iwate, Japan (Email: gaoshouyi888@yahoo.co.jp).

M. Saito is a Professor in the Department of Design and Media Technology, Graduate School of Engineering, Iwate University, Morioka, Iwate, Japan (Email: mitsugu@iwate-u.ac.jp).

Rapidly locating these areas is a prerequisite for establishing effective transportation routes for rescue operations in the aftermath of such disasters. With escalating concerns about a potential Nankai Trough megathrust earthquake [4], it has become increasingly important to explore more efficient and timely methods for assessing road accessibility and critical infrastructure conditions in disaster-affected areas. Relevant studies reveal that the restoration of road accessibility following the 2011 Great East Japan Earthquake was remarkably slow [5].

Given the limitations of traditional and alternative methods, there is growing interest in leveraging satellite data and GIS for detecting inundated areas. Satellite imagery offers a scalable solution, providing high spatial and temporal resolution for monitoring large areas in near real time. Recent advancements in high-resolution remote sensing satellites have enabled this technology to deliver valuable information in fields such as natural resource exploration [6], ecological conservation, and disaster prediction. Recognizing the potential of satellite technology, Japan has developed advanced systems for assessing disaster conditions using satellite data. Notably, the Strategic Innovation Promotion Program, led by the Cabinet Office, developed the Disaster Situation Analysis and Sharing System [7] in 2022. This system provides essential satellite data to government agencies and municipalities within 2 hours of a disaster, facilitating quicker decision-making and response efforts. Satellite imagery has proven invaluable for visualizing disaster-affected areas, especially after natural disasters like earthquakes and tsunamis, aiding post-disaster relief and recovery operations.

Moreover, traditional road navigation systems, such as Google Maps, may fail to detect passable routes following large-scale disasters. Therefore, utilizing satellite imagery to identify impassable roads and determine the most efficient routes to disaster areas via passable roads is crucial for rescue operations and infrastructure recovery. This capability has the potential to become an important tool for government agencies and private organizations in efficiently carrying out their work [8].

This research utilizes satellite data and GIS integration to delineate inundated areas and develop a system to identify the shortest transportation routes for aggregate supply (from quarries to disaster areas), which is essential for infrastructure restoration.

II. RESEARCH METHODS

A. Study Area

This study focuses on the coastal towns and cities of Miyagi Prefecture, which were severely impacted by the

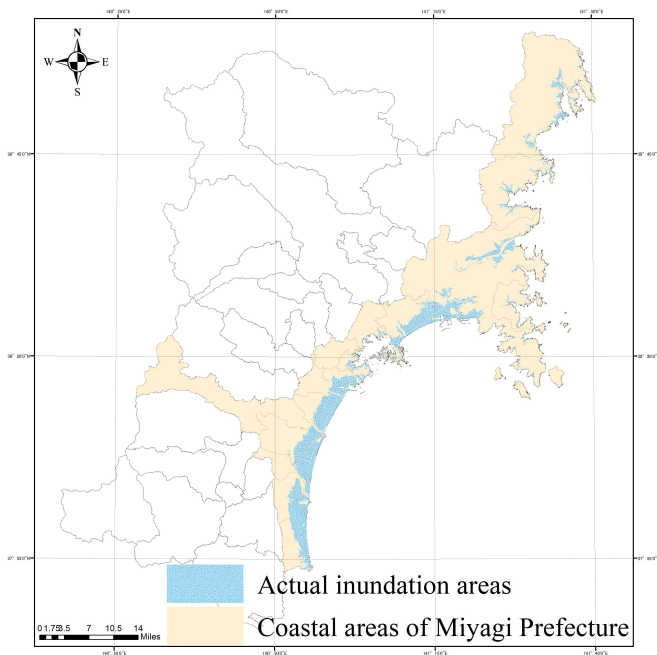


Fig. 1. Actual tsunami inundation areas and the affected cities and towns in Miyagi Prefecture.

widespread tsunami following the Great East Japan Earthquake on March 11, 2011. Figure 1 illustrates the actual tsunami-inundated areas and the affected cities and towns.

B. System

1) Hardware:

The computations were performed on a laptop PC equipped with a 12th Gen Intel® Core™ i7-12700H processor running at 2.70 GHz and 16 GB of memory (MSI Vector GP76 12UH).

2) Software:

The software used in this study includes ArcGIS version 10.8.1.14362 and Microsoft Office 2019, both running on the Windows 11 Professional operating system.

C. Research Materials

1) Polygon Data for the Tsunami Inundation Area after the 2011 Great East Japan Earthquake in Miyagi:

We confirmed the extent of tsunami inundation using GIS and referenced tsunami inundation maps provided by the Geospatial Information Authority of Japan [9].

2) Satellite Data:

We used satellite image data from Landsat 7 ETM+ [10] (observed on March 12, 2011) and MODIS/Terra Land [11] (observed on March 14, 2011).

3) Digital Elevation Model (DEM) Data of the Coastal Areas of Miyagi Prefecture:

We employed DEM data of the coastal areas in TIFF format for elevation analysis. The elevation range across these areas is -4.28 meters to 1365.29 meters [12].

4) Quarry Database:

We utilized data from the Current Status Survey of Quarries in the Tohoku Region, conducted by the Crushed Stone Research Group in 2021.

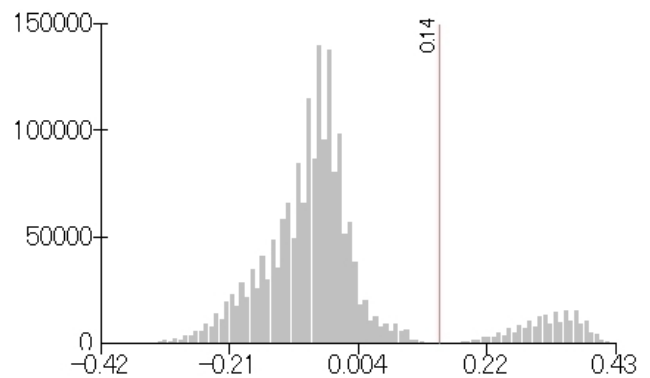


Fig. 2. Histogram of NDWI values.

5) National Digital Road Map Database (Miyagi Prefecture Primary Roads):

We used the National Digital Road Map Database Standard, Version 3.17 [13].

III. EXTRACTION OF INUNDATED AREAS

As outlined in the introduction, this methodology consists of two primary parts. The first involves extracting tsunami-inundated areas along the coast of Miyagi Prefecture using satellite imagery data, focusing on the aftermath of the Great East Japan Earthquake.

A. Extraction of Normalized Difference Water Index (NDWI) Values

The NDWI value is expressed by equation (1) [14].

$$NDWI = \frac{Green - NIR}{Green + NIR} \quad (1)$$

where the Green Band corresponds to the wavelength range of approximately 0.5~0.6 μm , and the NIR (near-infrared) Band corresponds to the wavelength range of around 0.7~1.3 μm .

Figure 2 shows the histogram of NDWI values (x-axis) and the number of data points (y-axis) for the inundated areas along the coast of Miyagi Prefecture as of March 12, 2011. Figure 3 presents the NDWI Distribution Map of the Coastal Areas of Miyagi Prefecture on the same date.

The histogram generated by the mode method is bimodal, suggesting that the NDWI value distribution includes both water and non-water areas. The minimum value in the valley between the peaks was set as the threshold for NDWI values [15].

Figure 4 displays the GIS image of the inundated area extracted using NDWI values.

B. Extraction of Land Surface Temperature (LST_{Day_1km}) Values

When a normally dry land surface becomes covered with water, its temperature changes [16]. Thus, we used land surface temperature data to extract the inundated area.

LST is calculated using the Generalized Split-Window method [17], which estimates surface temperature from the observed brightness temperatures T_{31} and T_{32} of MODIS data Bands 31 and 32 through equations (2) and (3):

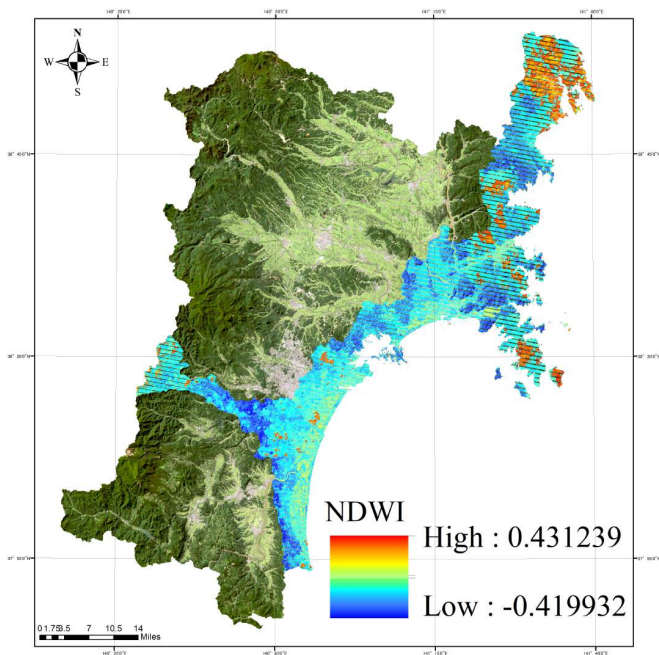


Fig. 3. NDWI distribution map of the coastal areas of Miyagi Prefecture on March 12, 2011.

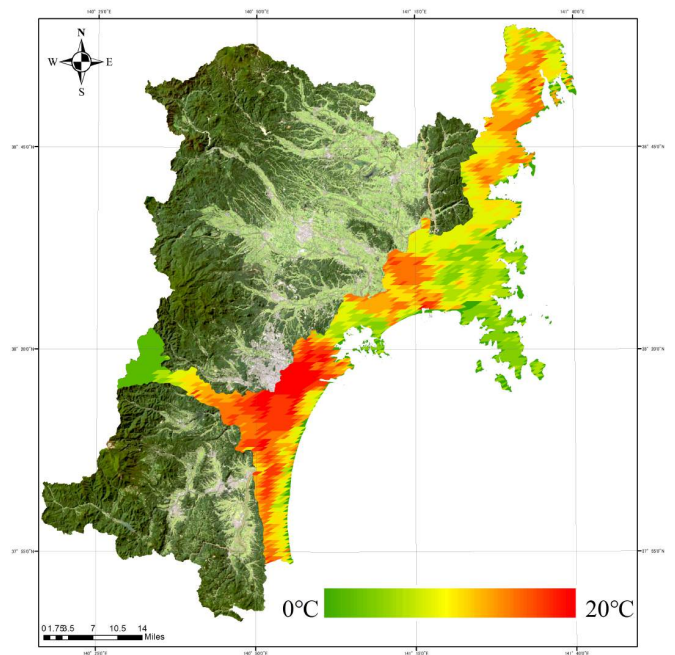


Fig. 5. LST distribution map of the coastal areas of Miyagi Prefecture on March 14, 2011.

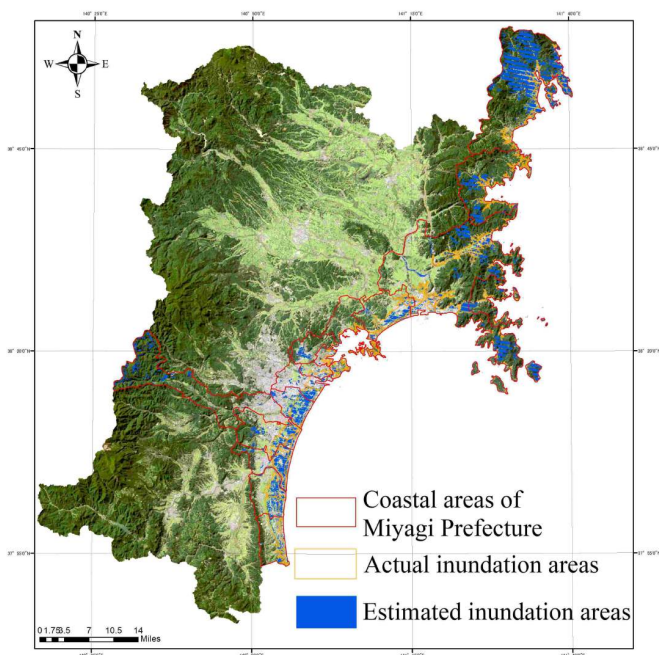


Fig. 4. Estimated inundation area extracted using NDWI values.

$$LST = \left(A_1 + A_2 \frac{1 - \epsilon}{\epsilon} + A_3 \frac{\Delta\epsilon}{\epsilon^2} \right) \frac{T_{31} + T_{32}}{2} + \left(B_1 + B_2 \frac{1 - \epsilon}{\epsilon} + B_3 \frac{\Delta\epsilon}{\epsilon^2} \right) \frac{T_{31} - T_{32}}{2} + C \quad (2)$$

where A_i is the regression coefficient ($i = 1, 2, 3$), B_i is the observation angle ($i = 1, 2, 3$), and C is the precipitable water.

$$\left. \begin{aligned} \epsilon &= 0.5(\epsilon_{31} + \epsilon_{32}) \\ \Delta\epsilon &= \epsilon_{31} - \epsilon_{32} \end{aligned} \right\} \quad (3)$$

where $\epsilon_{31}, \epsilon_{32}$ are the surface emissivities of MODIS Bands 31 and 32.

Based on the distribution of LST values along the coast of Miyagi Prefecture on March 14, 2011 (Fig. 5) and the temperature distribution trends near the actual inundation line, we hypothesized a threshold of 12°C for LST values and extracted areas with LST values below this threshold as inundated areas.

In this approach, the Manual Thresholding method is employed to visually inspect the distribution of LST values in regions where significant temperature differences are observed within the same terrain [18]. By focusing on the boundary where temperature variation becomes pronounced, we selected a specific LST value as the threshold. This threshold is manually set at the point where the temperature difference is noticeable, particularly in areas covered by debris (such as collapsed buildings or rubble) following the tsunami.

Figure 6 shows the GIS image of the inundated area extracted using LST values.

C. Extraction of Inundated Areas through Integrated Analysis of NDWI and LST Values

Using the two datasets of inundation areas derived from NDWI and LST values, we combined the extracted inundated areas with the GIS Union function to create a comprehensive representation. This process merged results from both indices, ensuring that all potential inundated areas identified by either NDWI or LST were included in the final dataset. The GIS Union function effectively resolves overlaps and discrepancies between these datasets, resulting in a unified and accurate depiction of the affected regions.

Figure 7 shows the GIS visualization of the combined inundation area, providing a clear and detailed spatial representation of the areas impacted by the tsunami.

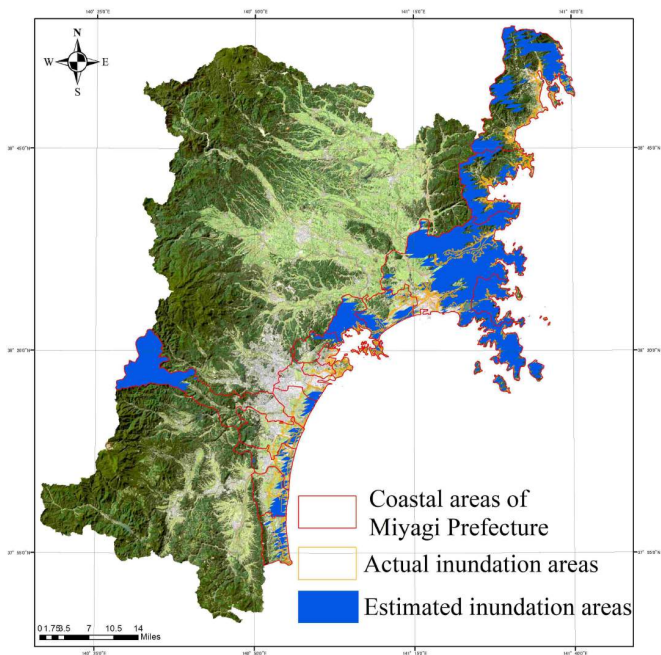


Fig. 6. Estimated inundation area extracted using LST values.

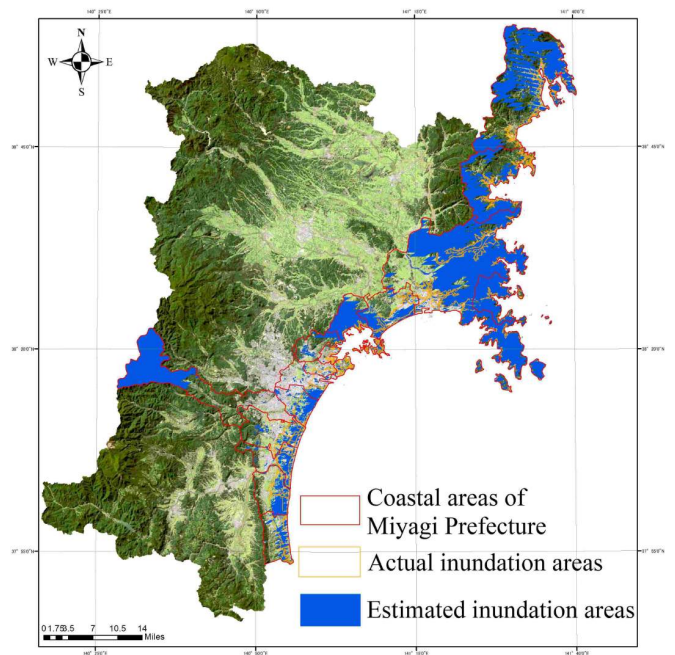


Fig. 7. Estimated inundation area extracted using NDWI and LST values.

D. Extraction of Snow-Covered Areas Using the Normalized Difference Snow Index (NDSI)

Since snow-covered surfaces may have been mistakenly included in the inundated areas extracted using NDWI and LST values, we attempted to extract NDSI values using Landsatt 7 ETM+ (Band 2 Green and Band 5 SWIR). Snow-covered areas exhibit high reflectance in the Green Band and low reflectance in the Shortwave Infrared (SWIR) Band. NDSI values were calculated using equation (4) [19]:

$$NDSI = \frac{Green - SWIR}{Green + SWIR} \quad (4)$$

where the Green Band corresponds to a wavelength range of approximately 0.5~0.6 μm, and the SWIR Band corresponds to a wavelength range of about 1.1~3.0 μm.

Figure 8 shows the distribution of NDSI values in the coastal areas of Miyagi Prefecture on March 12, 2011, as calculated in ArcGIS. Snow-covered areas were determined to have NDSI values of 0.4 or higher [20].

Figure 9 shows the GIS visualization of snow-covered areas identified through the application of NDSI values, highlighting regions with significant snow accumulation extracted based on a predefined NDSI threshold. This method effectively delineates snow-covered areas, distinguishing them from other land features such as water bodies and bare ground.

E. Removal of Snow-Covered Areas from Inundated Areas through Integrated Analysis of NDWI and LST Values

After utilizing the integrated analysis of NDWI and LST values to extract inundated areas, we removed the snow-covered areas identified by NDSI values.

Figure 10 illustrates the inundated areas after excluding the snow-covered areas from the NDWI and LST values. The earthquake occurred in early March, a period when

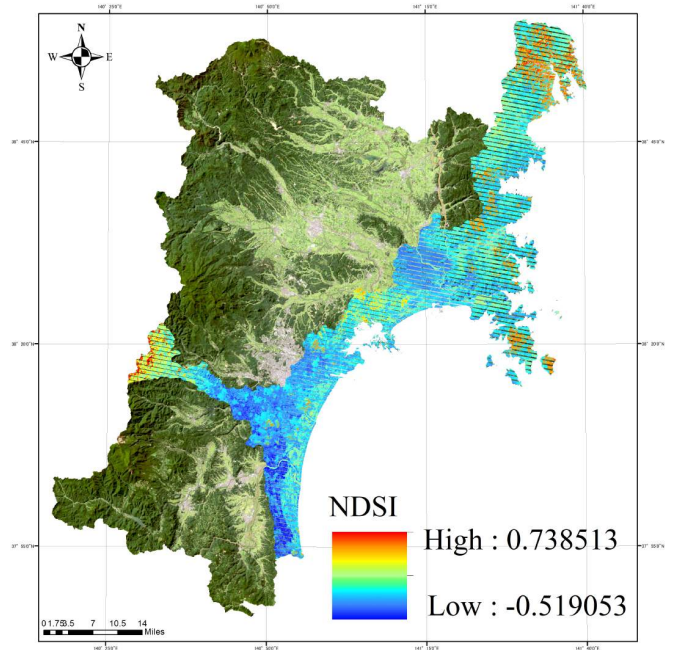


Fig. 8. NDSI distribution map of the coastal areas of Miyagi Prefecture on March 12, 2011.

significant snow accumulation is still present in the Tohoku region, particularly at higher elevations [21]. Snow-covered areas typically exhibit lower surface temperatures, and failing to account for them during the extraction of inundated areas using LST values can lead to inaccuracies. However, this step can be omitted in future disaster analyses unless the event occurs during winter or other snowy periods. If a tsunami disaster occurs outside of snowy seasons, it would not be necessary to exclude snow.

F. Research Findings on Estimated Inundated Areas

The results of tsunami-inundated area extraction, using an integrated analysis of NDWI, LST, and NDSI values,

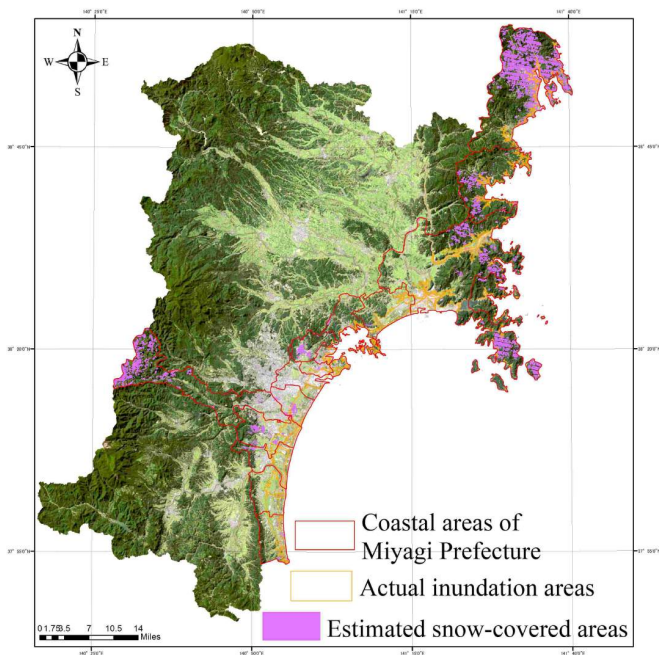


Fig. 9. Snow-covered area extracted using NDSI values.

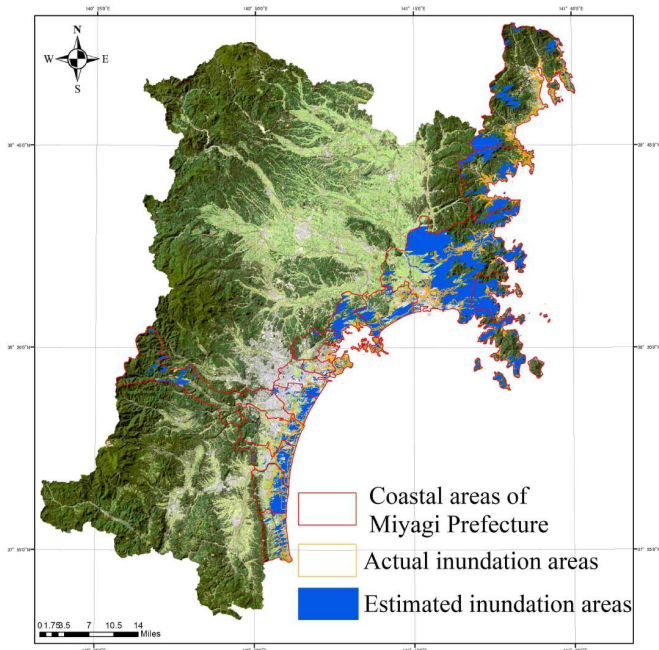


Fig. 10. Estimated inundation area by excluding snow-covered areas using integrated NDWI and LST values.

demonstrate a significant improvement in the accuracy of water body identification.

1) Challenges in Water Body Detection and Improvement with NDWI and LST Values Integration:

In the study area, collapsed buildings, vegetation, and vehicles posed challenges for water body detection. Using NDWI or LST values alone resulted in an extraction accuracy of only 40%, while their combination doubled accuracy to around 80%. Using the government-provided actual inundation area of 307.69 km² [9], and referring to Fig. 7, the extracted blue inundated areas align well with government provided actual inundated areas (yellow frames), particularly in the southeastern coastal plains of Miyagi Prefecture.

2) Issues of Erroneous Water Extraction and Improvement with NDSI Values:

Despite improved accuracy, erroneous extractions persisted, primarily in high-altitude areas with snow cover. As shown in Table I, integrating NDWI and LST values enhanced detection but also resulted in the largest area of misidentified water bodies. Referring to Fig. 5, these errors were concentrated in low-temperature mountainous regions, indicating snow-related misclassification. Incorporating NDSI reduced erroneous extractions by nearly 50% (Fig. 11), making water body identification more reliable. While the extraction ratio within actual inundated areas decreased slightly, the elimination of false positives significantly improved accuracy.

3) Practical Implications and Future Improvements:

Given the resolution limitations of free medium-to-low-resolution resolution satellite data, this methodology remains valuable for rapid disaster assessment. Future research should incorporate higher-resolution datasets and advanced algorithms to further improve accuracy [22].

Additionally, as satellite images were taken hours after the tsunami, some water may have receded, affecting boundary accuracy. Earlier image acquisition could enhance detection performance.

4) Conclusion and Significance of the Proposed Methodology:

This study highlights the benefits of multi-source data integration for disaster mapping. The combined NDWI, LST, and NDSI values approach enhances tsunami impact identification, improving disaster response efficiency. This method not only strengthens Japan’s disaster resilience but also provides a scalable framework for other tsunami and flood-prone regions.

This aspect is a fundamental component of this research’s thematic significance.

IV. CONSTRUCTION OF AGGREGATE TRANSPORT ROUTES DURING DISASTERS

The second part of this methodology focuses on the construction of aggregate transport routes during disasters, aiming to establish the most efficient routes between aggregate supply quarries and essential infrastructure in need of immediate repair after a large-scale tsunami inundation event.

A. Designing an Optimized Aggregate Transport Route Model

Using the inundated areas extracted from satellite data after the earthquake, the DEM data of the coastal areas of Miyagi Prefecture, the National Digital Road Map Database (Miyagi Prefecture Primary Roads), and the quarry database, we designed a model to construct aggregate transportation routes (Fig. 12).

B. Excluding High-Elevation Errors to Extract Inundated Areas Using DEM Data

On the basis of the outlined methodology, we used NDWI, LST, and NDSI satellite data to identify tsunami-inundated areas following the 2011 Great East Japan Earthquake. Figure 10 shows a combined visualization of satellite imagery

TABLE I
STATISTICS OF TSUNAMI-INUNDATED AREAS EXTRACTED USING VARIOUS SATELLITE DATA AFTER THE 2011 GREAT EAST JAPAN EARTHQUAKE.

	Extracted inundation area (km^2)	Inundation area covered by the actual inundation area (km^2)	Erroneously extracted inundation area (km^2)	Extraction rate relative to the actual tsunami inundation area
NDWI	377.69	122.58	443.62	40%
LST	969.66	117.07	1043.21	38%
NDWI + LST	1198.28	229.82	1046.33	81%
NDWI + LST - NDSI	640.75	199.72	549.00	65%

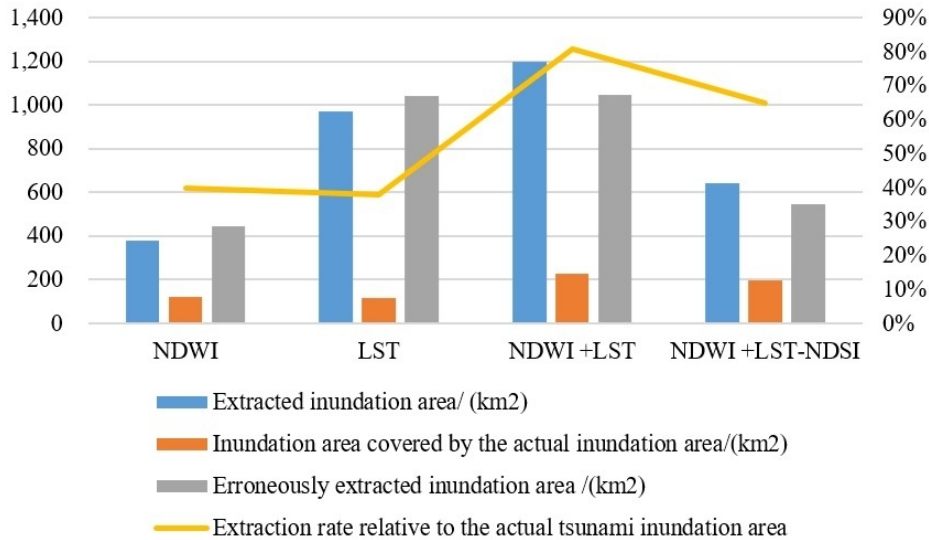


Fig. 11. Bar chart of tsunami-inundated area statistics extracted using different satellite data.

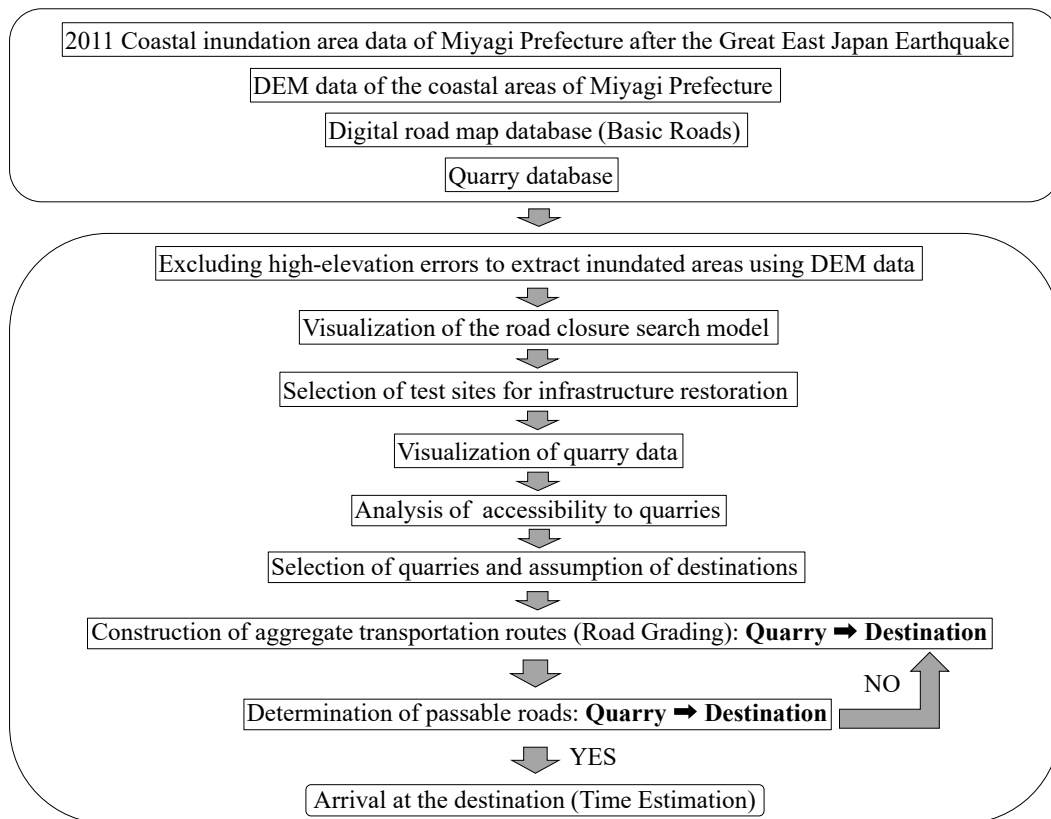


Fig. 12. Model for aggregate transportation routes.

and inundated areas, revealing that some higher-elevation mountainous areas were mistakenly classified as inundated.

This misclassification likely occurred because tsunami inundation typically affects lower-lying plains, highlighting the

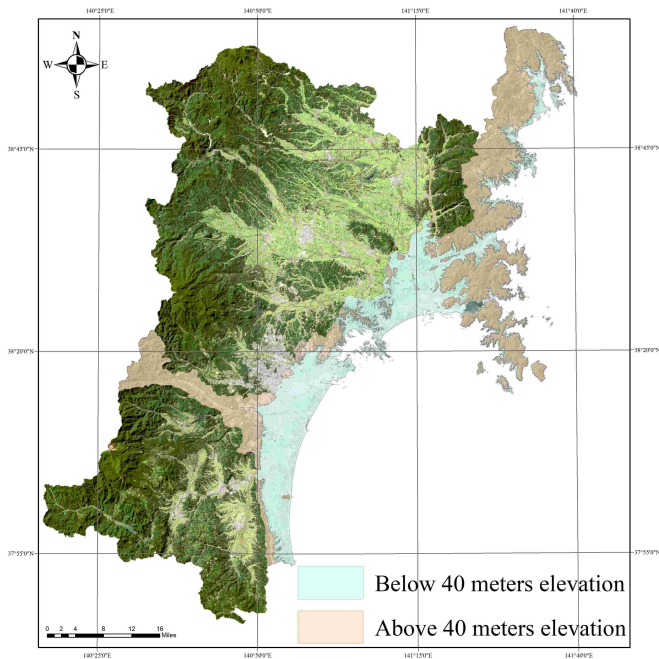


Fig. 13. Elevation area above and below 40 m in the coastal areas of Miyagi Prefecture.

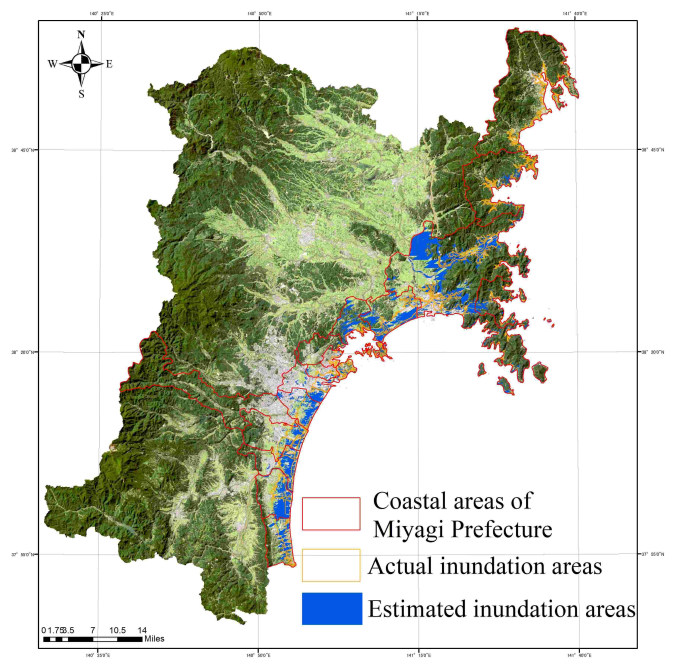


Fig. 14. Estimated inundation area by clipping using 40 m threshold.

importance of excluding higher elevations when determining inundated areas [23].

For elevation analysis, we utilized DEM data from the coastal areas of Miyagi Prefecture, Japan, and established a 40 m threshold, which represents the highest recorded tsunami inundation level in Tohoku [24], to enhance classification accuracy.

Figure 13 illustrates the two areas above and below the 40 m elevation. By using the area above 40 m to clip the previously extracted tsunami inundation zones, we produced a more accurate inundation map, as shown in Fig. 14.

C. Impassable Road Search Model

The maximum run-up height of the tsunami in Miyagi Prefecture during the earthquake was 34.7 m [25]. Therefore, assuming that areas more than 40 meters above sea level will remain unaffected by tsunami inundation, we used GIS to combine the estimated tsunami-inundated areas less than 40 meters above sea level with Miyagi Prefecture’s primary road network to visualize impassable roads (Fig. 15).

D. Selection of Test Sites for Infrastructure Restoration

Based on the information presented in “Miyagi’s Journey to Recovery” [26], we selected seven public infrastructure districts that suffered significant damage during the earthquake. Table II lists these districts along with their corresponding location coordinates.

E. Visualization of Miyagi Prefecture Quarry Data

The GIS system was employed to visualize the quarry database. Figure 16 presents an example of this visualization, displaying the location of the quarry along with the percentage distribution of various types of crushed stone production.

In this step, the necessary aggregates can be determined based on the types of public infrastructure requiring urgent

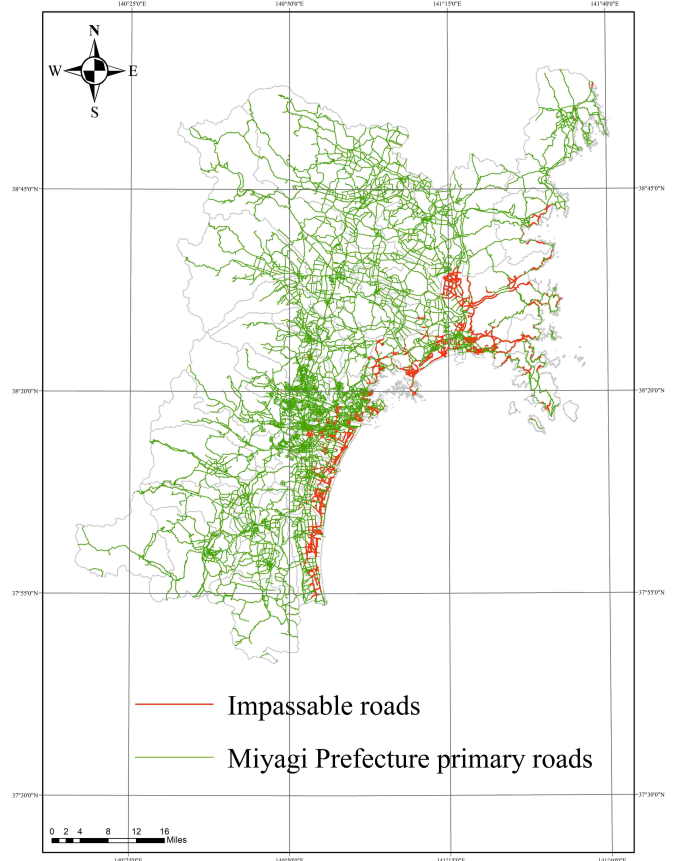


Fig. 15. Impassable road search model.

assistance, allowing for the selection of quarries capable of providing the needed raw materials.

F. Analysis of Transportation Roads from Quarries to Target Areas in Miyagi Prefecture

When calculating the distance from quarries to disaster-affected areas, the Euclidean Distance tool in ArcGIS was

TABLE II
SELECTION OF TEST SITES FOR INFRASTRUCTURE RESTORATION.

Case study	Experimental infrastructure restoration site	Coordinates
I	Kesennuma City, Minamimachi coastal area (seawall)	38°52'36.7"N, 141°35'22.5"E
II	Natori City, Iwanuma City area (Sendai Airport)	38°08'26.3"N, 140°55'16.4"E
III	Sendai City, Wakabayashi Ward, Arahama area (prefectural road Route 10)	38°13'09.5"N, 140°59'03.8"E
IV	Higashimatsushima City, Nobiru area (Nobiru Station)	38°22'45.7"N, 141°09'26.6"E
V	Onagawa Town, Onagawa area (Onagawa Station, Onagawa port, surrounding roads)	38°26'46.1"N, 141°26'39.5"E
VI	Ishinomaki City, Nakase area (West Naito Bridge)	38°25'51.4"N, 141°18'41.8"E
VII	Minamisanriku Town, Shizugawa area (along National Route 45)	38°41'15.1"N, 141°27'24.1"E

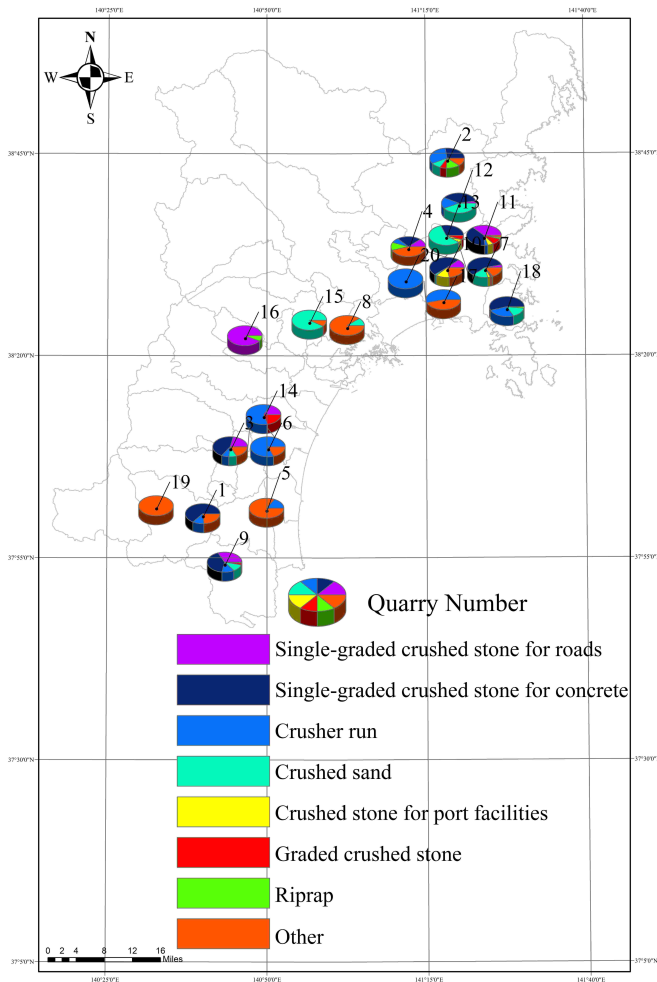


Fig. 16. Data visualization of quarries in Miyagi Prefecture.

utilized. Since the coordinate system is based on geographic coordinates (latitude and longitude), calculating the distance between two points requires converting latitude and longitude into planar coordinates [27]. This is necessary because geographic coordinates represent positions on a spherical surface rather than straight-line distances on a plane. To ensure that the calculated distances have linear units, the geographic coordinate data were first projected into a planar coordinate system. The projected coordinate system used in this study was JGD 2000 Japan Zone 10 [28], which represents Japan and uses meters as units.

The Euclidean distance on a two-dimensional plane is represented by the straight-line distance between points (x_1, y_1) and (x_2, y_2) , as expressed in equation (5) [29]:

$$d = \sqrt{(x_2 - x_1)^2 + (y_2 - y_1)^2} \quad (5)$$

where (x_1, y_1) is the coordinate of the first point and (x_2, y_2) is the coordinate of the second point.

Using the Euclidean distance tool, we calculated the distances between each selected public infrastructure site and the corresponding quarries, ensuring efficient planning for restoration efforts.

G. Optimization of Aggregate Transportation Route

Figure 17 shows the aggregate transportation route from the nearest quarry, while Table III presents the model results for aggregate transportation routes from the nearest quarry to each of the seven selected infrastructure restoration districts.

By organizing the optimized aggregate transportation routes hierarchically and referencing the speed limits for different road categories from the Nationwide Digital Road Map Database Standard Edition (Version 3.17) [13], we can calculate the estimated travel time. This estimation is achieved by applying the appropriate average speeds based on road types.

H. Example of Case Study II

Using the Natori/Iwanuma District as the destination and Quarry 6 as the nearest source, the optimal aggregate transportation route was determined based on the estimated Euclidean distance. Figure 18 illustrates the aggregate transportation route from Quarry 6. The system calculated the total transportation distance to be 12,716.52 meters, with an estimated travel time of approximately 24.74 minutes.

I. Example of Case Studies VII-1 and VII-2

Quarry 12 is the nearest quarry to the Shizugawa area in Minamisanriku Town. However, the shortest route crosses an inundated and impassable area (Fig. 19). Consequently, the system selects an alternative aggregate transportation route that avoids these impassable roads (Fig. 20). Figure 21 illustrates the aggregate transportation route from Quarry 2. By utilizing Quarry 2, which is not the nearest in terms of Euclidean distance, the system calculates the distance to the destination and compares the transportation distances on passable roads. This approach facilitates the identification of the most optimal aggregate transportation route, considering both time and distance. The calculated transportation distances are 30,129.13 meters from Quarry 12 and 21,685.86 meters from Quarry 2, with estimated travel times of approximately 42.80 minutes and 29.79 minutes, respectively.

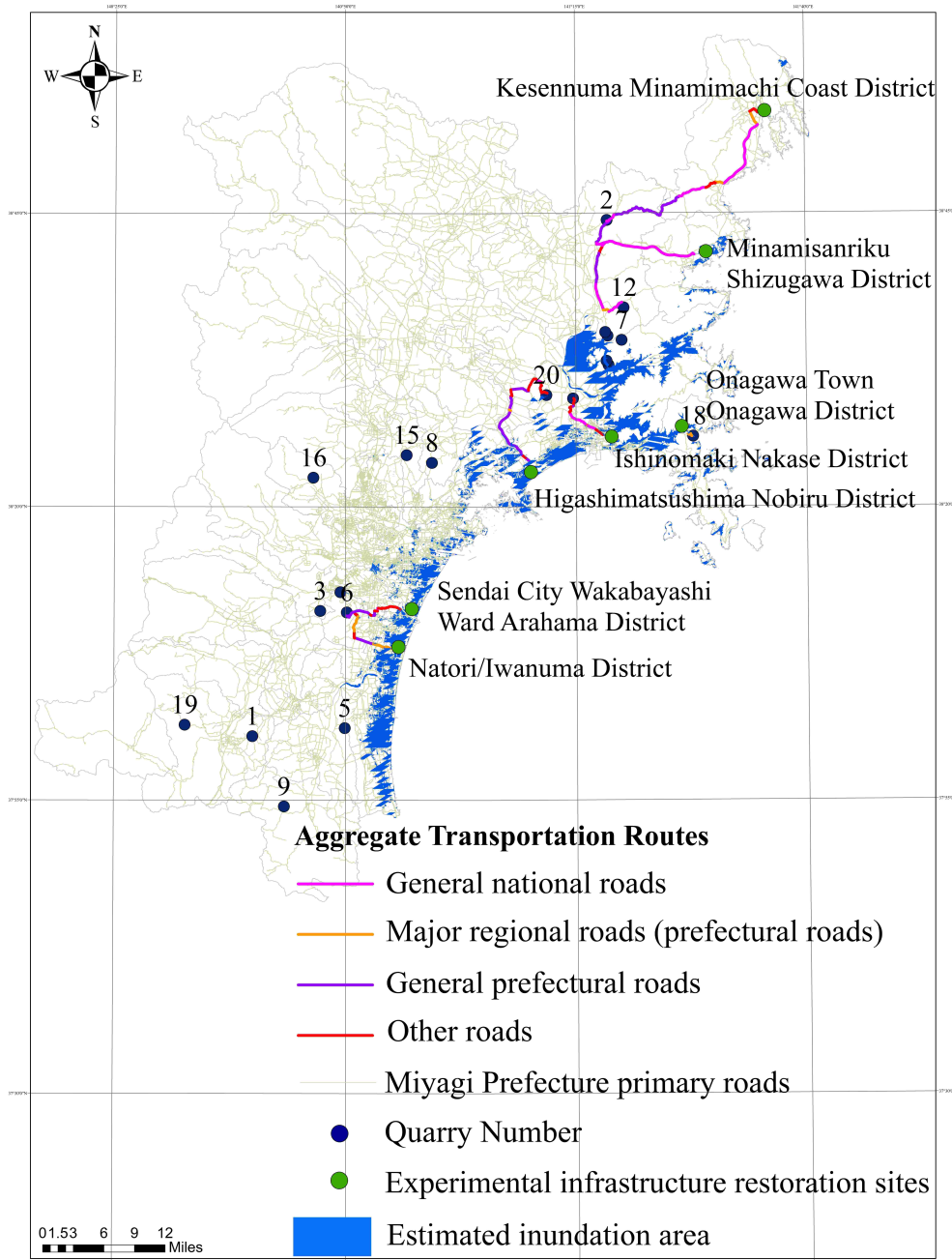


Fig. 17. Visualization of aggregate transportation routes.

TABLE III
OPTIMIZED AGGREGATE TRANSPORTATION ROUTES AND ESTIMATED TRAVEL TIMES.

Case study	Starting point	Destination	Optimizing aggregate transport route	Optimal aggregate transport distance (m)	Estimated time required (min)
I	Quarry 2	Kesennuma City, Minamimachi coastal area (seawall)	Feasible	39299.57	65.94
II	Quarry 6	Natori City, Iwanuma City area (Sendai Airport)	Feasible	12716.52	24.74
III	Quarry 6	Sendai City, Wakabayashi Ward, Arahama area (prefectural road Route 10)	Feasible	10817.02	25.96
IV	Quarry 20	Higashimatsushima City, Nobiru area (Nobiru Station)	Feasible	23883.64	54.47
V	Quarry 18	Onagawa Town, Onagawa area (Onagawa Station, Onagawa port, surrounding roads)	Not feasible	945.46	1.42
VI	Quarry 17	Ishinomaki City, Nakase area (West Naito Bridge)	Feasible	9509.99	19.42
VII-1	Quarry 12	Minamisanriku Town, Shizugawa area (along National Route 45)	Feasible	30129.13	42.80
VII-2	Quarry 2	Minamisanriku Town, Shizugawa area (Along National Route 45)	Feasible	21685.86	29.79

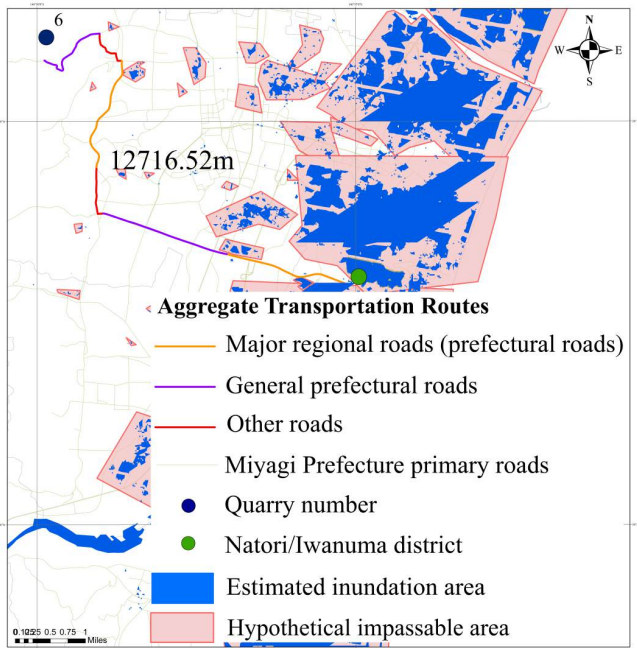


Fig. 18. Example of case study II.

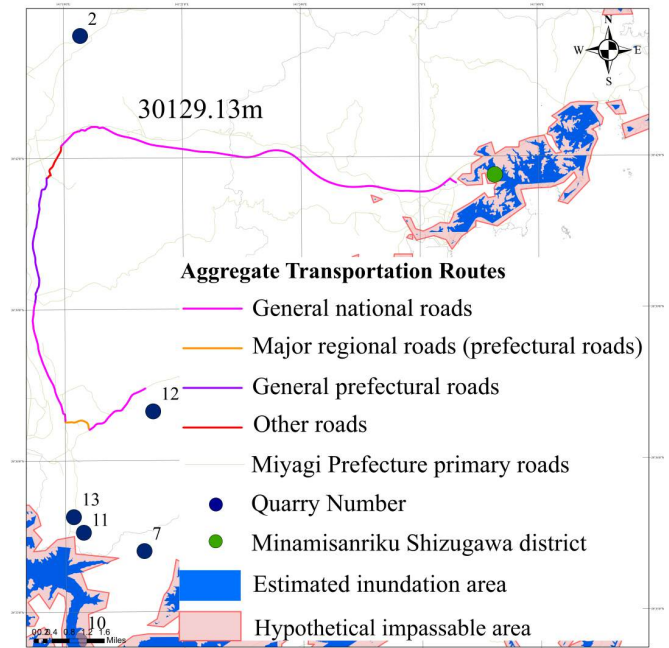


Fig. 20. Example of case study VII-1.

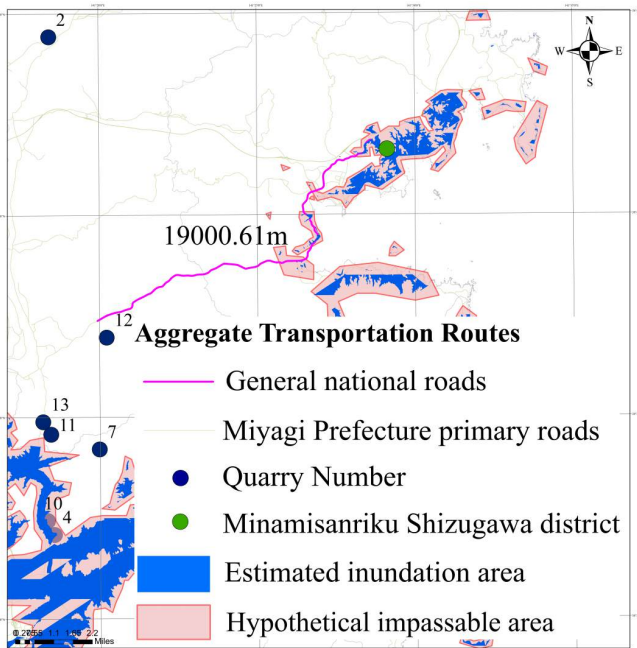


Fig. 19. Example of case study VII (Impassable section).

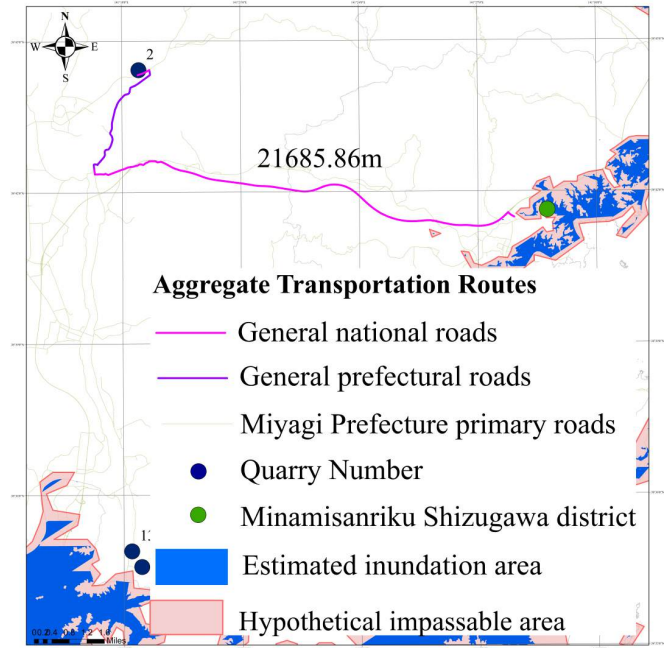


Fig. 21. Example of case study VII-2.

V. CONCLUSION

This study aimed to develop optimized passable routes connecting quarries that supply aggregate resources to public infrastructure in urgent need of repair and restoration following earthquakes and tsunami-induced inundation disasters. To achieve this, we employed an integrated approach combining satellite imagery analysis and GIS tools to provide a systematic and data-driven method for post-disaster logistics planning.

1) Contribution of the Proposed System:

This study introduced a novel system for optimizing aggregate transportation routes in the aftermath of a natural disasters. Efficient infrastructure repair is essential not

only for saving lives but also for reviving socio-economic functions, particularly following large-scale disasters such as tsunamis and widespread flooding. The system enables real-time assessment of road network conditions, allowing for the identification of the shortest and most efficient routes from quarries to disaster-affected areas. By integrating satellite imagery with GIS tools, it effectively extracts data on impassable roads, ensuring uninterrupted material transportation under disaster-induced constraints. The system has been empirically tested by analyzing aggregate transportation routes to seven destinations. The results indicate that the system can dynamically generate optimal routes, estimate required travel times, and effectively enhance the speed and cost-efficiency of post-disaster recovery operations.

2) Limitations and Challenges:

Despite its effectiveness, the study faced inherent limitations of satellite data, primarily due to resolution constraints and susceptibility to cloud cover during image acquisition. These factors led to frequent misidentifications in inundation-prone areas, posing challenges in constructing reliable aggregate transportation route models. Addressing these challenges requires integrating higher-resolution satellite data, advanced image processing techniques, and machine learning algorithms to enhance the accuracy of inundation area delineation. These improvements will contribute to more precise identification of passable roads, ultimately leading to greater efficiency in disaster response and faster infrastructure restoration efforts.

3) Future Implications:

The findings highlight the urgent need for innovative solutions in disaster management and emphasize the importance of technology-driven approaches in ensuring efficient and timely recovery efforts. Future improvements, such as integrating higher-resolution satellite data and advanced computational models, will further enhance the proposed system's practical applicability.

Overall, this study contributes to enhancing Japan's disaster resilience and presents a scalable disaster assessment framework that could be adapted for use in other tsunami and flood-prone regions worldwide.

ACKNOWLEDGMENT

I would like to express my heartfelt gratitude to Professor Noriaki Endo, formerly of the Graduate School of Integrated Science at Iwate University. He provided invaluable support in the use of GIS software and offered substantial guidance throughout the journal submission process. His generous support and invaluable guidance have been essential to the progress of this study. Additionally, I extend my sincere thanks to the Japan Digital Road Map Association for supplying the National Digital Road Map Database Standard, Version 3.17. These data have been instrumental in ensuring the accuracy and development of our research analysis.

REFERENCES

- [1] Japan Meteorological Agency (n.d.): *Earthquakes in Japan*, Accessed June 18, 2024, Retrieved from JMA <https://www.jma.go.jp/>
- [2] Ministry of Land, Infrastructure, Transport and Tourism, Disaster Prevention Japan: *Expert Committee on Large-Scale Flood Countermeasures, Disaster Information*, Accessed September 10, 2024, Retrieved from <https://www.bousai.go.jp>
- [3] LiDAR vs Traditional Surveying: *A Clash of Technologies, Aerial Precision Drones*, Accessed October 25, 2023, Retrieved from <https://www.aerial-precision.com>
- [4] Okada, Y., & Kato, N: "Understanding the Tsunami Threat from the Nankai Trough," *Journal of Disaster Research*, 11(6), 1058–1066, 2016
- [5] Shouyi Gao, Noriaki Endo, and Mitsugu Saito, "Regional and Altitudinal Differences on Road Usage Recovery in Aomori Prefecture Following the 2011 Tohoku Earthquake," *IAENG International Journal of Computer Science*, vol. 51, no. 11, pp1880-1885, 2024
- [6] NASA. (n.d.): *NASA's Earth Observing System*, Accessed November 2023, Retrieved from <https://earthdata.nasa.gov>
- [7] Kazushima, I., Tanaka, H., Takatsuki, Y., & Nakata, A: *Satellites, Drones, and SocialMedia, Rapid Assessment of Damage, Nikkei Computer*, Accessed October 2021, March 2, Retrieved from <https://xtech.nikkei.com/atcl/nxt/mag/nc/18/022400216/022400004/>
- [8] Smith, D: "The Role of Infrastructure in Disaster Recovery," *International Journal of Disaster Risk Reduction*, 5, 21–30, doi: 10.1016/j.ijdr.2013.04.004, 2013
- [9] Geospatial Information Authority of Japan: *Ministry of Land, Infrastructure, Transport and Tourism, Details of Inundation Areas*, Accessed October 25, 2024, Retrieved from <http://fukkou.csis.u-tokyo.ac.jp/dataset/show/id/1110>
- [10] U.S. Geological Survey (USGS): *Landsat 7 ETM+ Surface Reflectance Level-2 Science Product, (2011)*, Accessed 2021, Retrieved from <https://earthexplorer.usgs.gov>
- [11] NASA EOSDIS Land Processes DAAC: *MODIS/Terra Land Surface Temperature and Emissivity Daily L3 Global 1 km SIN Grid*, Accessed 2021, Retrieved from <https://doi.org/10.5067>
- [12] National Institute of Geography of Japan (GSI Japan): *Digital Elevation Model (DEM) Data, (2024)*, Accessed April 2024, Retrieved from <https://www.gsi.go.jp>
- [13] Japan Digital Road Map Association: *Nationwide Digital Road Map Database Standard Edition (Version 3.17), (2021)*, Accessed May 2024, Retrieved from <https://drm.jp/english/>
- [14] Gao, H: NDWI: "A new method for detecting water bodies," *Remote Sensing of Environment*, 58(3), 325–333. doi:10.1016/S0034-4257(96)00067-7, 1996
- [15] Fukumoto, M: "Identification of Water Intake Start Period for Paddy Fields Using Sentinel-2 Satellite Data," *System Agriculture (J. JASS)*, 35(2), 15–23, 2019
- [16] Tamagawa, I., Yamada, M., Ikebuchi, S., & Mitsuta, Y: "On the Relationship between Surface Moisture Content and Surface Temperature Variations," *Annual Report of the Disaster Prevention Research Institute*, Kyoto University, 31B (1), 1988
- [17] Wan, Z. M., & Dozier, J: "A generalized split-window algorithm for retrieving land-surface temperature from space," *IEEE Transactions on Geoscience and Remote Sensing*, 34(4), 892–905. doi:10.1109/36.508406, 1996
- [18] Weng, Q., Lu, D., & Schubring, J: "Estimation of land surface temperature–vegetation abundance relationship for urban heat island studies," *Remote Sensing of Environment*, 89(4), 467–483, 2004
- [19] Crane, R. G., & Anderson, M. R: "Satellite discrimination of snow/cloud surfaces," *International Journal of Remote Sensing*, 5(1), 213–223, 1984
- [20] Dozier, J: "Spectral signature of alpine snow cover from the Landsat Thematic Mapper," *Remote Sensing of Environment*, 28, 9–22, 1984
- [21] Tohoku Regional Development Bureau: *Snowfall and snow depth in the Tohoku region, (2021)*, Accessed September 2024, Retrieved from <https://www.thr.mlit.go.jp/>
- [22] Zhang, Z., & Zhang, X. . ARE-Net: "An Improved Interactive Model for Accurate Building Extraction from High-Resolution Remote Sensing Images," *Remote Sensing*, 15(18), 4457. <https://doi.org/10.3390/rs15184457>, 2023
- [23] Goto, K., & Imamura, F: "Numerical modeling of tsunami waves and its application to long-term hazard assessment," *Journal of Disaster Research*, 2(1), 69-76, 2007
- [24] Nobuhito Mori, Tomoyuki Takahashi, and the 2011 Tohoku Earthquake Tsunami Joint Survey Group: "Nationwide Post Event Survey and Analysis of the 2011 Tohoku Earthquake Tsunami," *Coastal Engineering Journal*, ISSN, 1793-6292. doi:10.1142/S0578563412500015, 2016
- [25] Geospatial Information Authority of Japan (GSI): *Report on the 2011 Tohoku Earthquake and Tsunami, Analysis of Tsunami Inundation, (2011)*, Accessed November 2024, Retrieved from http://www.gsi.go.jp/BOUSAI/h23_tohoku.html
- [26] Miyagi Prefecture Disaster Recovery Headquarters: *Steps Towards Reconstruction, (2023)*, Accessed August 2024, Retrieved from <https://www.pref.miyagi.jp/site/ej-earthquake/ayumi.html>
- [27] Esri. (n.d.): *Understanding Euclidean distance analysis*, Accessed November 2024, Retrieved from <https://pro.arcgis.com/en/pro-app/latest/tool-reference/spatial-analyst/understanding-euclidean-distance-analysis.htm>
- [28] Geospatial Information Authority of Japan: "Japan Geodetic Datum 2000 (JGD2000)," 2002. [Online]. Accessed November 2024, Retrieved from <https://www.gsi.go.jp/>
- [29] R. O. Duda, P. E. Hart, and D. G. Stork, *Pattern Classification*, 2nd ed. New York, NY, USA: *Wiley-Interscience*, 2001